Detuned secondary instabilities in three-dimensional boundary-layer flow

Detuned secondary instabilities in three-dimensional boundary-layer flow

Antoine Jouin[1,2], Nicola Ciola[1,2], Stefania Cherubini[1], and Jean Christophe Robinet[2*]
Dipartimento di Meccanica, Matematica e Management, Politecnico di Bari ,
Via Re David 200, 70125 Bari, Italy and
Laboratoire DynFluid, Arts et Métiers Institute of Technology
151 Bd de l'Hopital, 75013 Paris, France
(Dated: May 9, 2024)

In this work, we apply a new formulation for capturing detuned secondary instabilities. This formulation, based on two-dimensional stability analysis coupled with a Bloch waves formalism originally described in Schmid *et al.* [1], allows to consider high-dimensional systems resulting from several repetitions of a spatially periodic unit, by solving an eigenproblem of much smaller size. Secondary instabilities coupling multiple periodic units can be thus retrieved. The method is applied on the secondary stability of a swept boundary-layer flow subject to stationary cross-flow vortices. Two distinct detuned secondary instabilities are retrieved. The first one, obtained for a detuning factor $\epsilon = 0.35$ and reaching a maximum growth rate for streamwise wavenumber $\alpha_v = 0.087$, was already found in the work of Fischer and Dallmann [2]. The second instability is obtained for streamwise independent modes and small detuning factor $\epsilon = 0.08$. The corresponding mode presents large-wavelength oscillations, arising from a characteristic beating phenomenon. The physical origin of these two secondary instabilities has been investigated by varying the amplitude of the primary disturbance: for the latter instability, reminiscent of a type-III mode, the unstable branch continuously deforms as the amplitude is increased; whereas, a change of topology of the spectrum is observed for the $\alpha_v = 0$ mode.

I. INTRODUCTION

Transition to turbulence is a crucial problem of great technical interest in fluid mechanics. A successful approach for studying it consists in dividing the process into several stages. An initial stage, denoted as primary instability, can be investigated through linear stability theory, either modal or non-modal [3]. These analyses yield structures representative of the primary instability mechanisms such as, for example, Tollmien-Schlichting (TS) waves for channel or boundary-layer flows [4], cross-flow vortices for swept flows [5], gravity waves in stratified flows [6] or streaks in the case of non-modal mechanisms [7]. The previous list is far from being exhaustive as the relevant structures strongly depend on the flow configuration and the case considered.

These flow structures are likely to further destabilise, resulting in the second stage of the transition process. Investigation of this second stage is possible through secondary stability theory, established through the seminal works of Orszag and Patera [8] and Herbert [9] on two-dimensional TS waves in wall-bounded flows. Precisely, in the simplest cases, secondary stability theory is based on a Floquet analysis of a secondary base flow constructed as the superposition of an initial laminar flow and a primary disturbance previously identified. Notably, in channel and boundary layer flows, the exponential growth of small three-dimensional disturbances, observed experimentally and in numerical simulations, was explained as a secondary instability of two-dimensional TS waves [8, 9]. Following these seminal works, the theory was applied to numerous other configurations such as, for example, streaks in boundary-layer [10] or cross-flow vortices in swept flows [2, 11], leading to breakthroughs in the identification of the underlying mechanisms of transition to turbulence.

Peculiar long-wavelength modes can be observed in several flow configurations, usually coupling multiple length scales, such as the flow over superhydrophobic surfaces with moving interfaces [12], large arrays of vortices [13] or vortex pairings in mixing layers [14]. The origin of such long-wavelength, detuned modes can be investigated by means of secondary instability of primary modes. In this article we use a new formulation for secondary stability analysis based on the association of a local two-dimensional stability analysis and a Bloch waves formalism. This formulation is based on the mathematical framework proposed by Schmid *et al.* [1] for the primary stability analysis of fluid systems consisting of a spatially periodic array of n identical units. A similar framework has already been employed in the field of vibration analysis to study rotationally symmetric systems like bladed disks (see Olson *et al.* [15] for a review in this context). This method allows to compute multi-modal fluid instabilities, i.e., modal solutions that are spatially periodic over the array of n units, despite not being periodic over individual units, without solving the whole eigenvalue problem. Using this formalism, secondary stability analyses can be carried out on very large systems, allowing

* jean-christophe.robinet@ensam.eu

to capture modes with small detuning factors spanning several wavelengths of the primary disturbance or resonances. We present here an application of this framework to secondary stability theory of a swept boundary layer subject to stationary cross-flow modes. In this case the spatial periodicity, necessary for the application of the method, results from the periodicity of the primary disturbance, and not from the spatial recurrence of a geometric feature as for the examples provided in Schmid *et al.* [1]. The case of the swept boundary layer subject to stationary cross-flow modes has been chosen due to previous observation of long-wavelength structures in numerical and experimental studies. In fact, in a DNS study of such a flow case [16], detuning of the secondary instability appeared, but it was not further investigated. Moreover, long wavelength coherent flow structures have been experimentally reported by [17], but their physical origin remained unclear. Finally, to the authors' knowledge, despite the extensive literature on the secondary instabilities in swept boundary layers [2, 11, 17–19], no study has considered yet the simultaneous secondary instability of a large number of cross-flow vortices. Moreover, for small spanwise wavelength instabilities, a direct comparison can be made with results from the Floquet analysis of Fischer and Dallmann [2], allowing a validation of the results. The outline of the remainder of the paper is as follows. The mathematical framework described in Schmid *et al.* [1] will be adapted for the study of secondary instabilities in §II. The results and discussion on the secondary stability of the swept boundary layer are contained in §III. The main findings are summarised in §IV.

II. MATHEMATICAL FRAMEWORK

Let us consider a general, time-evolving system of the form:

$$\frac{\partial \mathbf{Q}}{\partial t} = \mathbf{F}\left[\mathbf{Q}(\mathbf{x},t)\right] \tag{1}$$

where $\mathbf{Q}$ is the state vector, $\mathbf{F}$ a non-linear operator and $\mathbf{x} = (x, y, z)$ is the spatial coordinates vector, with x being the streamwise, y the wall-normal, and z the spanwise direction. The flow is decomposed into a base flow $\mathbf{Q}_0\,(y)$, assumed to be locally parallel, and a small primary disturbance $\mathbf{q}_1(\mathbf{x}, t)$, such that $\mathbf{Q}(\mathbf{x}, t) = \mathbf{Q}_0(y) + \mathbf{q}_1(\mathbf{x}, t)$. Substituting the previous decomposition into Eq.(1) and neglecting nonlinear terms results in the following system for the perturbation:

$$\frac{\partial \mathbf{q}_1}{\partial t} = \mathbf{A}\mathbf{q}_1 \tag{2}$$

with $\mathbf{A}$ the Jacobian of the system. Assuming an ansatz of the form $\mathbf{q}_1(\mathbf{x}, t) = \tilde{\mathbf{q}}_1(y) \exp\left[i(\alpha x + \beta z - \omega t)\right]$, modal and non modal stability analysis [3] can be performed, identifying specific waves of interest, with (α, β) the spatial and ω the temporal wavenumber. Notice that the primary instability analysis is carried out in a temporal framework, so that α, β are real quantities whereas $\omega = \omega_r + i\omega_i$ is complex.

From there, following Herbert [9], the secondary base flow $\mathbf{Q}_1$ is defined as the superposition of the primary disturbance of interest $\mathbf{q}_1$, with amplitude A, and the primary base flow $\mathbf{Q}_0$, such that $\mathbf{Q}_1(\mathbf{x}, t) = \mathbf{Q}_0(y) + A\mathbf{q}_1(\mathbf{x}, t)$. We also introduce a new Galilean coordinate system (x_v, y, z_v) normal to the wave vector $\mathbf{k} = (\alpha, \beta)^T$ of the primary disturbance moving with phase speed $c = \omega_r/||\mathbf{k}||$ in the z_v-direction. The passage from one coordinate system to the other can be performed through the following Squire transform: $x_v(t) = \beta/||\mathbf{k}||x - \alpha/||\mathbf{k}||z$ and $z_v(t) = \alpha/||\mathbf{k}||x + \beta/||\mathbf{k}||z - ct$. In this new frame, the secondary base flow $\mathbf{Q}_1(y, z_v)$ is stationary, streamwise independent and $2\pi/||\mathbf{k}||$-periodic in the spanwise direction z_v. In the wave-oriented reference frame, the flow is decomposed into the secondary base flow $\mathbf{Q}_1(y, z_v)$ and a small secondary perturbation $\mathbf{q}_2(x_v, y, z_v, t)$ such as $\mathbf{Q}(x_v, y, z_v, t) = \mathbf{Q}_1(y, z_v) + \mathbf{q}_2(x_v, y, z_v, t)$. This formulation requires the shape assumption to be valid. Potentially, the base flow for secondary stability analysis can be retrieved by other means, such as parabolised stability equations or direct extraction from a numerical simulation. The key point is to guarantee the spatial periodicity of the secondary base flow on the sub-units. Modal secondary perturbations are assumed:

$$\mathbf{q}_2(x_v, y, z_v, t) = \tilde{\mathbf{q}}_2(y, z_v) \exp\left(i\alpha_v x_v + \sigma t\right) \tag{3}$$

with α_v and $\sigma = \sigma_r + i\sigma_i$ being respectively the (real) streamwise wavenumber and the (complex) temporal wavenumber, σ_r being the growth rate and σ_i being the circular frequency of the modes.

In the classical theory of secondary stability, Floquet analysis would be applied on the secondary base flow $\mathbf{Q}_1$. Instead, we consider a fluid system composed of the repetition in the spanwise direction z_v of the secondary base flow $\mathbf{Q}_1$ over n sub-units of length $2\pi/||\mathbf{k}||$. The Navier-Stokes equations are then linearised around the $2\pi/||\mathbf{k}||$-periodic base flow $\mathbf{Q}_1(y, z_v)$. The ansatz for the secondary disturbance is introduced, yielding a two-dimensional local stability problem with $2\pi/||\mathbf{k}||$-periodic coefficients. The equations for the stability problem linearised around a two-dimensional stationary base flow $\mathbf{Q}_1(y, z_v) = [U_1(y, z_v), V_1(y, z_v), W_1(y, z_v)]^T$ can be found in Loiseau [20] and are reproduced here for the sake of clarity:

$$
\begin{cases}
\sigma\tilde{u}_2 + i\alpha_v U_1\tilde{u}_2 + V_1\partial_y\tilde{u}_2 + W_1\partial_{z_v}\tilde{u}_2 + \tilde{v}_2\partial_y U_1 + \tilde{w}_2\partial_{z_v}U_1 = \\
\qquad -i\alpha_v\tilde{p} + \dfrac{1}{Re}(\partial_{yy} + \partial_{z_v z_v} - \alpha_v^2)\tilde{u}_2 \\
\sigma\tilde{v}_2 + i\alpha_v U_1\tilde{v}_2 + V_1\partial_y\tilde{v}_2 + W_1\partial_{z_v}\tilde{v}_2 + \tilde{v}_2\partial_y V_1 + \tilde{w}_2\partial_{z_v}V_1 = \\
\qquad -\partial_y\tilde{p} + \dfrac{1}{Re}(\partial_{yy} + \partial_{z_v z_v} - \alpha_v^2)\tilde{v}_2 \\
\sigma\tilde{w}_2 + i\alpha_v U_1\tilde{w}_2 + V_1\partial_y\tilde{w}_2 + W_1\partial_{z_v}\tilde{w}_2 + \tilde{v}_2\partial_y W_1 + \tilde{w}_2\partial_{z_v}W_1 = \\
\qquad -\partial_{z_v}\tilde{p} + \dfrac{1}{Re}(\partial_{yy} + \partial_{z_v z_v} - \alpha_v^2)\tilde{w}_2 \\
i\alpha_v\tilde{u}_2 + \partial_y\tilde{v}_2 + \partial_{z_v}\tilde{w}_2 = 0
\end{cases}
\tag{4}
$$

where Re is the Reynolds number. Performing a classical linear stability analysis of a system of this size yields a prohibitive computational cost. However, this task can be tackled at an affordable cost using the framework described by Schmid *et al.* [1]. For the sake of completeness, the method will be quickly described in the following. The first step consists in reordering the system, which is partitioned into n smaller systems, each one corresponding to a sub-unit. Mathematically, the disturbance equations can be recast under the following form:

$$
\frac{\partial}{\partial t}\begin{pmatrix} \mathbf{q}_2^{(0)} \\ \mathbf{q}_2^{(1)} \\ \vdots \\ \mathbf{q}_2^{(n-1)} \end{pmatrix} = \underbrace{\begin{pmatrix} \mathbf{A}^{(0)} & \mathbf{A}^{(1)} & \dots & \mathbf{A}^{(n-1)} \\ \mathbf{A}^{(n-1)} & \mathbf{A}^{(0)} & \dots & \mathbf{A}^{(n-2)} \\ \vdots & \vdots & & \vdots \\ \mathbf{A}^{(1)} & \mathbf{A}^{(2)} & \dots & \mathbf{A}^{(0)} \end{pmatrix}}_{\mathbf{A}'} \underbrace{\begin{pmatrix} \mathbf{q}_2^{(0)} \\ \mathbf{q}_2^{(1)} \\ \vdots \\ \mathbf{q}_2^{(n-1)} \end{pmatrix}}_{\mathbf{q}_2}
\tag{5}
$$

with $\mathbf{A}'$ the Jacobian associated to the full secondary stability problem, which is composed of the matrices $\mathbf{A}^{(0)}$ and $\mathbf{A}^{(j)}$ (for $j = 0, ..., n-1$) describing respectively the dynamics in a sub-unit and the coupling interactions between sub-units. The secondary disturbance state vector in the j^{th} sub-unit is denoted as $\mathbf{q}_2^{(j)}$. The Jacobian matrix $\mathbf{A}'$ is block-circulant due to the specific n-periodic nature of the system and can become a block-diagonal matrix $\hat{\mathbf{A}}$ through the similarity transformation:

$$
\mathbf{P}^H\mathbf{A}'\mathbf{P} = \mathrm{diag}(\hat{\mathbf{A}}^{(0)}, \hat{\mathbf{A}}^{(1)}, ..., \hat{\mathbf{A}}^{(n-1)}) \equiv \hat{\mathbf{A}}
\tag{6}
$$

The transfer matrix $\mathbf{P}$ can be found analytically as:

$$
\mathbf{P} = \mathbf{J} \otimes \mathbf{I}
\tag{7}
$$

with $\mathbf{J}$ a matrix such as $\mathbf{J}_{j+1,k+1} = \rho_j^k/\sqrt{n}$ for $j, k = 0, ..., n-1$ and $\rho_j = \exp(2i\pi j/n)$ the j^{th} of the n roots of unity. The symbol $\otimes$ denotes the usual Kronecker product and $\mathbf{I}$ the identity matrix. With this transformation, the linear stability problem has been reduced to the study of n smaller sub-systems characterised by the matrices $\hat{\mathbf{A}}^{(j)}$. Hence, the full spectrum of the matrix $\mathbf{A}'$ can be found merging the n spectra of $\hat{\mathbf{A}}^{(j)}$ for $j = 0, ..., n-1$. Similarly, provided $\mathbf{v}_j$ is an eigenvector of $\hat{\mathbf{A}}^{(j)}$, the eigenfunctions of the full system can be retrieved and take the form $[\mathbf{v}_j, \rho_j\mathbf{v}_j, \rho_j^2\mathbf{v}_j, ..., \rho_j^{n-1}\mathbf{v}_j]^T$ for $j = 0, ..., n-1$. In the case of nearest-neighbour coupling, rather common in many applications, the Jacobian $\mathbf{A}'$ reduces to a block-tridiagonal matrix. Only a three-unit system $\mathbf{A}^{(0)}, \mathbf{A}^{(1)}, \mathbf{A}^{(2)}$ needs to be discretized and processed, significantly reducing the complexity and computational cost of the method. A sensitivity study of the method with respect to the nearest-neighbour coupling hypothesis, as well to the number of subunits considered, is carried out in the Appendix.

Notice that the argument θ_j of the root-of-unity ρ_j acts as a phase shift between the different sub-units: the farther it is from 0 (or 2π), the more desynchronised the secondary mode is. Thus, the eigenfunction $\mathbf{v}_j$, after each sub-unit, is phase shifted by $\theta_j = \arg(\rho_j) = 2\pi j/n$, meaning that after $n_j = 2\pi/\theta_j = n/j$, (here $j = 1, ..., n-1$) sub-units, the cumulative phase shift will exceed 2π, giving an estimate of the effective fundamental period of the eigenfunction of the full system. Associated with this number of coupled sub-units, the fundamental wavenumber of the mode can be retrieved and is equal to $\beta_v = 2\pi/(2\pi n_j/||\mathbf{k}||) = j||\mathbf{k}||/n$.

The connection with Floquet analysis and the corresponding detuning factor ϵ can be thus specified. In the wave-oriented frame, the secondary base flow is periodic with wavenumber $\beta_v^0 = ||\mathbf{k}||$ in the z_v direction. After Fourier expanding the base flow in this direction (see [3], for instance) the secondary disturbance has the following modal expansion:

$$\mathbf{q}_2(x_v, y, z_v, t) = e^{\sigma t} e^{i\alpha_v x_v} \sum_m \hat{\mathbf{q}}_m(y) e^{i(m+\epsilon)||k||z_v}. \tag{8}$$

where $\epsilon = \gamma_i/||\mathbf{k}||$, γ_i being the imaginary part of the classical Floquet exponent γ. The fundamental wavenumber ($m = 0$) of the resulting mode is thus $\beta_v = \epsilon||\mathbf{k}||$, which, after equating with the expression of β_v previously obtained for the $j-$th eigenmode with root-of-unity ρ_j, gives $\epsilon = 1/n_j = j/n$. Reintroducing the detuning factor into the Floquet modal expansion yields:

$$\mathbf{q}_2^{(j)}(x_v, y, z_v, t) = e^{\sigma t} e^{i\alpha_v x_v} e^{ij\frac{||k||}{n} z_v} \sum_m \hat{\mathbf{q}}_m(y) e^{im||k||z_v} \tag{9}$$

$$= e^{\sigma t} e^{i\alpha_v x_v} e^{ij\frac{||k||}{n} z_v} \tilde{\mathbf{q}}(y, z_v) \tag{10}$$

for $j = 0, ..., n-1$, where the Bloch theorem for the n sub-units is retrieved.
Comparing the computational cost of the Bloch wave method to that of a limited ($O(10)$) number of Floquet computations with different detuning factors, one can conclude that the total Cpu time is approximately equivalent. Thus, there is not a direct computational advantage of using such a method instead of Floquet analysis.
However, in the present framework, the eigenproblem is solved using a two-dimensional base flow, without needing to develop and truncate it in a Fourier series. This can be quite beneficial in the case of complex base flows (as mean flows), where using Fourier modes may not be convenient if the secondary base flow has been computed using a non-spectral method (e.g., a finite-difference numerical code). Of course, this would merely constitute a pragmatic advantage, while the two approaches are equivalent from both theoretical and computational point of view. Finally, since a large numbers of eigenmodes can be retrieved, the framework is also well suited for carrying out non-modal or resolvent analyses. These have not been described as the present article focuses on modal instabilites. For the full discussion, the reader is referred to Schmid *et al.* [1].

III. RESULTS

To illustrate the previous method, the secondary instability of stationary cross-flow vortices in a swept-boundary flow is investigated. This analysis extends and completes the work of Fischer and Dallmann [2], where long-wavelength instabilities were not investigated. All the stability results hereafter are obtained using a temporal approach ($\omega, \sigma \in \mathbb{C}$). The secondary stability problem is tackled considering the nearest-neighbour coupling assumption (see the Appendix for a validation of this assumption). For both primary and secondary analyses, the stability problem is discretised with a spectral collocation method [21]. Wall-normal and spanwise directions are respectively discretised with a 64-points Chebyschev grid and a 64-points Fourier grid, respectively. The generalised eigenvalue problem is solved using a Krylov-Schur algorithm of the SciPy Python module coupled with a shift-and-inverse technique.

A. Primary stability analysis

In the following, we consider the incompressible flow over an infinite swept flat plate with an imposed negative pressure gradient (i.e. decreasing pressure in the chordwise direction). The laminar base flow $\mathbf{Q}_0 = [U_0(y), 0, W_0(y)]^T$ is modelled with a Falkner-Skan-Cook profile [22, 23]. Precisely, introducing f and g such that $U_0(y) = f'(y)\cos\theta$ and $W_0(y) = g(y)\sin\theta$, we have:

$$(2 - \beta_H)f''' + ff'' + \beta_H\left[1 - (f')^2\right] = 0 \tag{11}$$

$$(2 - \beta_H)g'' + fg' = 0, \tag{12}$$

where the Hartree dimensionless pressure-gradient parameter (β_H), the local sweep angle and the local Reynolds number are set respectively to $\beta_H = 0.630$, $\theta = 46.9°$ and $Re = Re_\delta = 826$. These parameters are taken directly from Fischer and Dallmann [2], and set to fit qualitatively experimental results from Müller [24]. Assuming wave-like solutions for the disturbances, modal stability analysis is performed for this configuration. Stationary disturbances maximising the temporal growth rate with respect to the streamwise and spanwise wavenumbers α and β are sought. Figure 1 exhibits the neutral curve of the primary instability. Since Squire's theorem is not valid for three-dimensional flows [25], the $\beta < 0$ plane was also investigated for the sake of completeness. The maximum growth rate for stationary

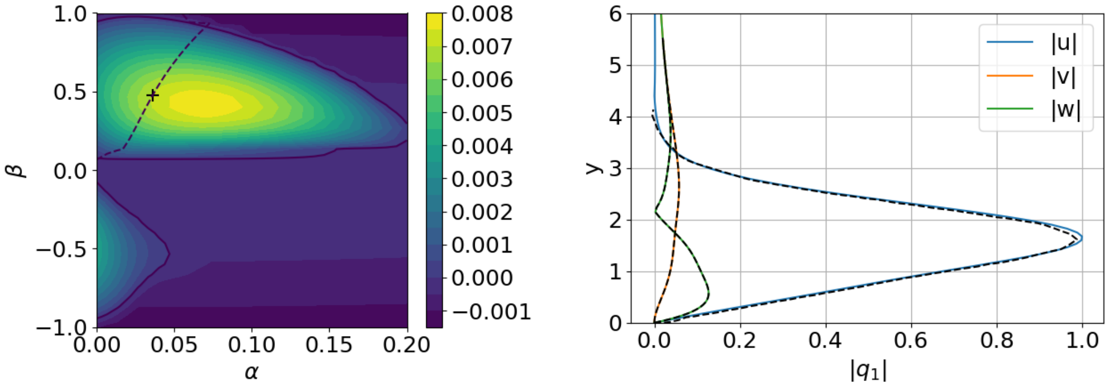

FIG. 1: Left: Neutral curve (black solid line $\omega_i(\alpha,\beta)=0$) of the swept boundary layer for $Re_\delta = 826$. The dashed line corresponds to stationary disturbances, i.e., $\omega_r(\alpha,\beta)=0$. Right: Absolute value of the eigenfunctions for $Re_\delta = 826$, $\alpha = 0.0361$ and $\beta = 0.4774$ ($\Psi = \arctan(\beta/\alpha) = 89.9^o$). The dashed lines are extracted from Fischer and Dallmann [2].

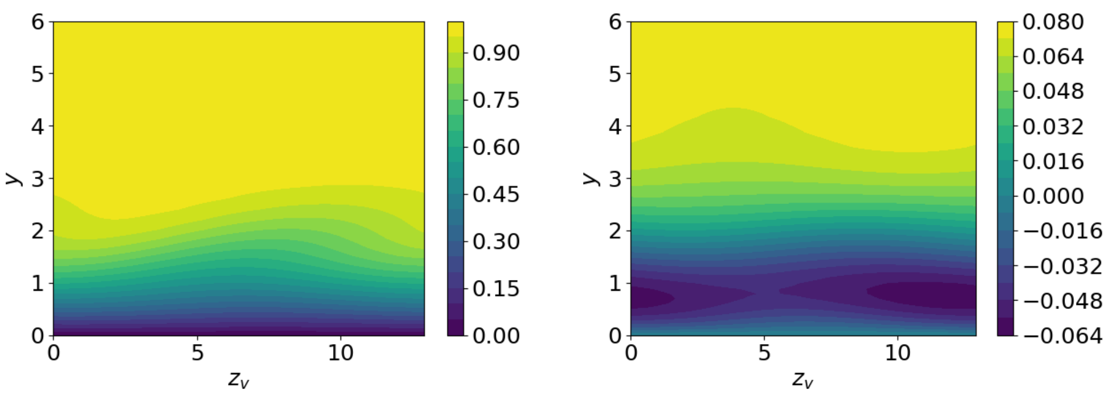

FIG. 2: Secondary base flow $U_1(y,z_v)$ (left) and $W_1(y,z_v)$ (right) in the wave-oriented reference frame, for one sub-unit. The wall-normal component V_1 is non-zero but is one order of magnitude smaller than W_1, thus it is not shown.

disturbances is reached for $(\alpha,\beta) = (0.0361, 0.4774)$. The eigenfunctions of this mode are displayed in figure 1 (right). A second instability region appears as well, albeit with lower growth rates and no stationary disturbances. The agreement with the results found in Fischer and Dallmann [2] is excellent.

B. Secondary stability analysis

Secondary stability of the flow is investigated using the framework described in §II. The secondary base flow is defined as $\mathbf{Q}_1(y,z_v) = \mathbf{Q}_0(y) + A\mathbf{q}_1(y,z_v)$ with $\mathbf{q}_1$ the disturbance with wavevector $\mathbf{k} = (\alpha,\beta) = (0.0361, 0.4774)^T$ in the original reference frame. The amplitude A is set as $A = 0.0789$ [2]. The resulting base flow on one sub-unit and in the wave-oriented reference frame is shown in figure 2. Qualitative validity of the shape assumption in this particular case is shown through comparison with experiments in Fischer and Dallmann [2]. Regarding the saturation amplitude, in a similar configuration, White and Saric [26] found a saturation amplitude of 19% for subcritical transition. This has been retrieved in the more recent work of Serpieri and Kotsonis [17] where, at worst, an N-factor of 3 was found, corresponding to a saturation amplitude of 20%. Returning to the study of White and Saric [26], in the case where the generated primary cross-flow vortices were supercritical, their amplitude only grew by a few percent before reaching saturation, in agreement with the chosen amplitude.

Secondary growth rate for the full system as a function of the streamwise wavenumber is displayed in figure 3.

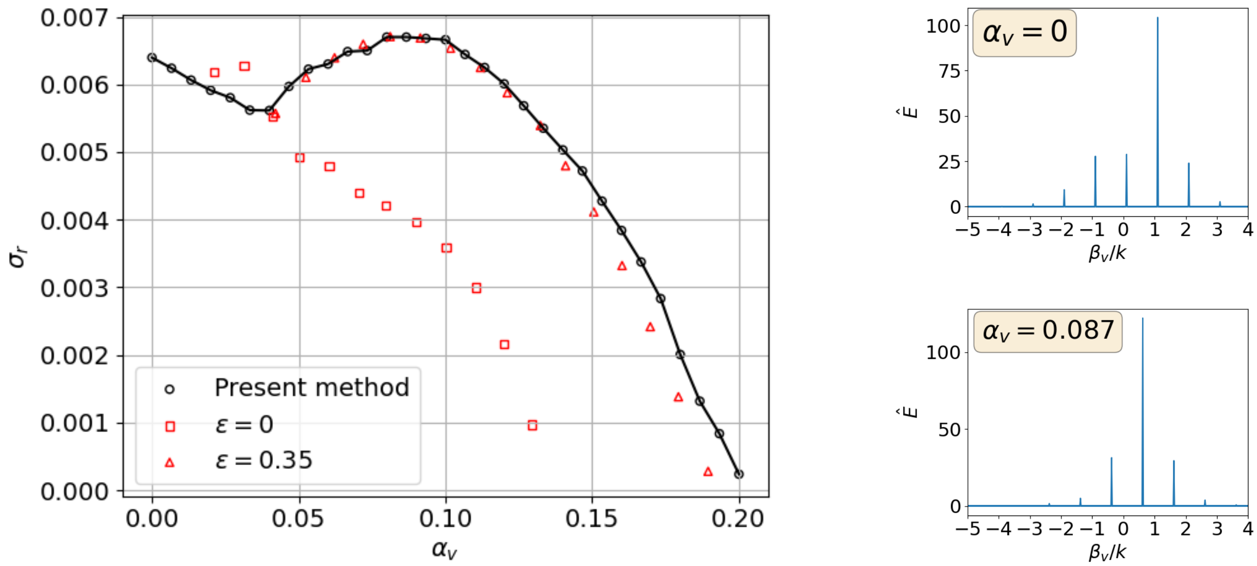

FIG. 3: Left: evolution of the secondary growth rate σ_r (black circles) as a function of the streamwise wavenumber α_v. A comparison is made with figure 8 of Fischer and Dallmann [2] (red symbols), where ϵ corresponds to the detuning factor of the Floquet analysis [2]. Right: Spatial Fourier spectra of the energy of the most unstable mode for $\alpha_v = 0$ (top) and $\alpha_v = 0.087$ (bottom).

Two modes appear to compete: the maximum growth rate $\sigma_r = 0.0068$ is reached for $\alpha_v = 0.087$ while streamwise independent perturbations ($\alpha_v = 0$) also display strong amplification with $\sigma_r = 0.0065$. A direct comparison can be made with figure 8 from Fischer and Dallmann [2], where Floquet analysis (on one sub-unit) is conducted for both harmonic modes and resonant modes with a detuning factor $\epsilon = 0.35$, where $\epsilon = \gamma_i/||\mathbf{k}||$ and γ_i is the imaginary part of the Floquet exponent γ, as discussed in II. Maximum growth rates are obtained for $\alpha_v = 0.03$ and $\alpha_v = 0.087$, respectively. The agreement with the $\epsilon = 0.35$ curve is good although some discrepancies are observed for the growth rates of harmonic modes. The Floquet analysis seems to overestimate the secondary growth rate in the range where small wavenumber modes are predominant.

The nature of the instabilities obtained in the new framework can be inferred inspecting the spatial Fourier energy spectra of the most unstable modes. These Fourier spectra, realised for the cases with $\alpha_v = 0$ and $\alpha_v = 0.087$, are shown in the right part of figure 3. The detuning factor can be identified, from the spectra, as $\epsilon = \beta_v/||\mathbf{k}||$ with β_v the wavenumber of the Fourier fundamental mode. Thus, the maximum at $\alpha_v = 0.087$ is associated to a detuned mode with $\epsilon = 0.35$, in agreement with Fischer and Dallmann [2]. For $\alpha_v = 0$, all the frequencies are almost multiples of $||\mathbf{k}||$, indicating a quasi-fundamental ($\epsilon = 0.08$) nature of the instability. It is also worth noticing the larger number of modes required to accurately describe the instability. The secondary perturbation is truly multi-modal with important coupling effects between sub-units. Notice that Fischer and Dallmann [2] missed this secondary mode, since the associated value of ϵ is very low, but still not zero.

The spectra for the system composed of $n = 50$ sub-units and for $\alpha_v = 0$ and $\alpha_v = 0.087$ are displayed in figure 4. A high number of sub-units corresponds to a (very) large system and allows a wide range of admissible spanwise wavenumbers. This explains the appearance of many branches within the spectra. The higher the number of sub-units, the more continuous these branches will be. Quasi-horizontal branches represent convective Squire modes and do not play a role in the asymptotic stability as they are always stable. The eigenvalues are coloured with the argument of their corresponding root-of-unity ρ_j. Brighter colours indicate important phase shift between sub-units and, thus, strong desynchronisation of the perturbation. For $\alpha_v = 0$, as expected, the spectrum is symmetric with respect to the $\sigma_i = 0$ axis. Two unstable branches are found: the most unstable one loops on itself. The second remains open ended. The maximum growth rate is reached for $\rho_4 = 0.87 + 0.48j$, corresponding to a phase shift $\theta = 29^o$ between the sub-units and indicating limited desynchronisation. The spectrum for $\alpha_v = 0.087$ is quite different. Two unstable branches are also observed. The first is marginally stable, and reaches a maximum growth rate for synchronised modes. The second is much more unstable and reaches a maximum for $\rho_{31} = -0.73 - 0.68j$, equivalent to a phase shift $\theta = -137^o$ and causing strong desynchronisation.

The most unstable modes are reconstructed for $\alpha_v = 0$ and $\alpha_v = 0.087$. Figure 5 displays the streamwise component

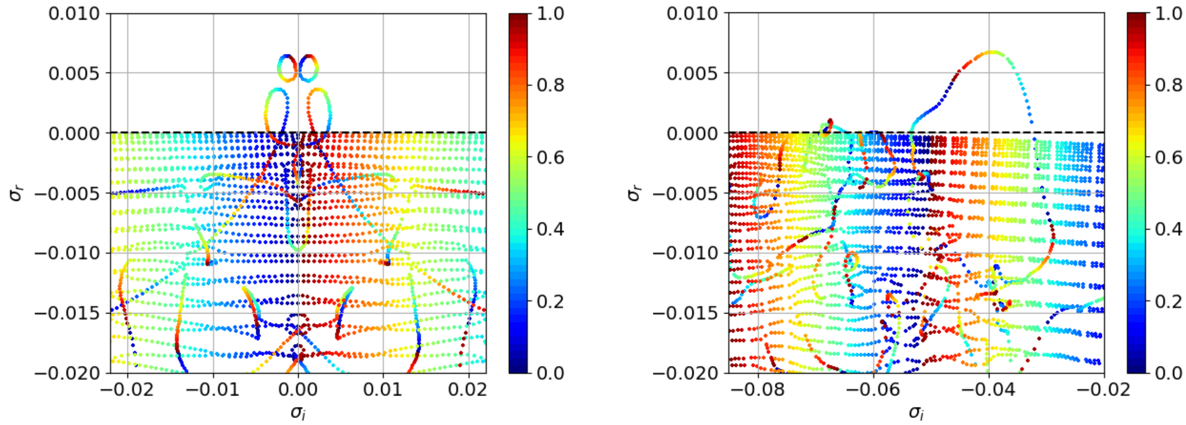

FIG. 4: Full spectra of the secondary stability problem for $Re_\delta = 826$, $A = 0.0789$, $n = 50$ and for $\alpha_v = 0$ (left) and $\alpha_v = 0.087$ (right). The full spectrum is constructed merging the n spectra of the sub-systems. The eigenvalues have been coloured by the argument of their respective root of unity: $z \in [0,1]$ such as $\rho = \exp(2i\pi z)$. The dashed line corresponds to the $\sigma_r = 0$ line.

of the disturbance velocity in the full domain while figure 6 exhibits the cross-flow velocities for a group of three sub-units. The streamwise velocity disturbance is one order of magnitude higher than the cross-flow components. The position of the maxima of the streamwise disturbance slightly varies across the sub-units, although it is approximately located on the upwelling of the wave pattern of the secondary base flow. The detuned behaviour can be observed in both modes: for $\alpha_v = 0$, approximately twelve sub-units are involved in large-wavelength oscillations; whereas only three contribute to the instability for $\alpha_v = 0.087$. The beating phenomenon observed for $\alpha_v = 0$ is characteristic of a superposition of functions with two close spatial wavelengths, one of these being the spatial wavelength of the primary cross-flow vortices which, in this context, acts as a forcing.

The cross-flow dynamics, displayed in figure 6 on a group of three sub-units, is less sensitive to unit-to-unit variation, likely due to the smaller magnitude of the components. The streamwise-independent mode displays counter-rotating vortices, which might be linked to either the lift-up effect or to a Gortler instability [27]. The latter is usually linked to curved walls, but it has been conjectured that the curvature of the base flow streamlines could have a similar effect on the instability of a boundary layer. Since the lift-up is usually a non-modal energy growth mechanism, while here we focus on modal instabilities, a Gortler-like instability can be a good candidate for explaining the onset of such counter-rotating vortices on top of the curved streamlines induced by the primary modes.
For $\alpha_v = 0.087$, the vortical structures are sensibly different. The vortices seem to arise from the roll-up of a shear layer. This might have been anticipated, since it has been shown that secondary instability of swept flows can be related to Kelvin-Helmholtz instabilities [19]. Furthermore, these secondary vortices are located on the edge of the boundary layer, in a region associated with strong wall-normal and spanwise shear layers. Ultimately, it appears that two distinct mechanisms are at play. The first is linked to streak instabilities, which push high-velocity fluid downwards near the walls while low-velocity fluid from the near-wall region is ejected higher in the boundary layer. The second instability mechanism is Kelvin-Helmholtz related, and generates secondary vortices through the roll-up of the shear layer located at the edge of the boundary layer.

In an effort to assess more precisely the instability nature of these two modes, a comparison can be made with the experimental work of Serpieri and Kotsonis [17], Serpieri [28] in which a POD decomposition of the laminar-turbulent transition on a swept wing was realised. The most energetic POD mode appeared to be streamwise-independent, with a shape similar to that found in the present analysis. Furthermore, it was characterised by a very low frequency in the [1Hz, 20Hz] range, in agreement with the frequency $f = 4$ Hz found here for the $\alpha_v = 0$ mode. However, no modulation of the mode has been observed as the POD was realised for only one cross-flow vortex. Figure 7 depicts the absolute value of the streamwise component of the disturbance. For $\alpha_v = 0.087$, the concentration of the streamwise velocity disturbance in the bottom part of the cross-flow vortices is reminiscent of a *type-III* instability [28]. The frequency $f = 154$ Hz obtained for this mode is smaller than the frequency range 350 Hz $\leq f \leq$ 550 Hz found by Serpieri [28] but still in good agreement with the frequency $f = 145$ Hz found by Fischer and Dallmann [2]. This type of mode is traditionally associated with interactions between primary stationary and travelling modes. The $\alpha_v = 0$ mode is quite interesting: the streamwise component of the perturbation is located on the upwelling of the cross-flow vortex which is characteristic of a *type-I* instability. The mode is also strongly correlated with the spanwise gradient

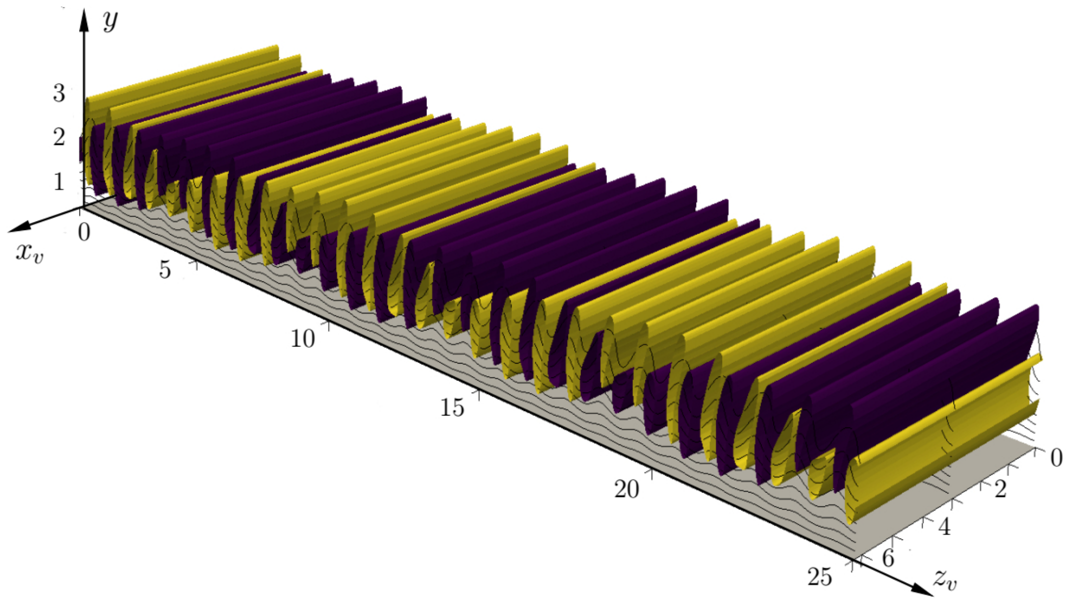

(a) $\alpha_v = 0$, $n = 25$

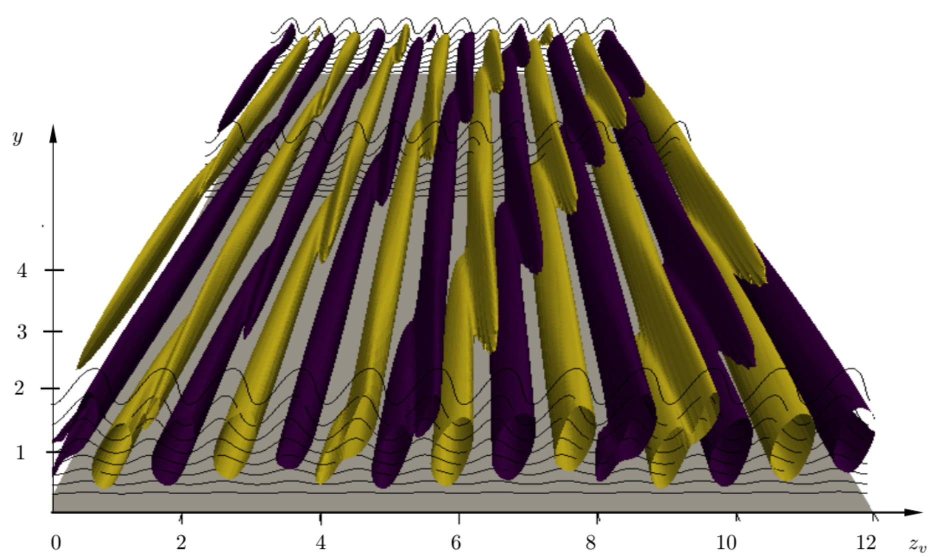

(b) $\alpha_v = 0.087$, $n = 12$

FIG. 5: Three dimensional views of the streamwise velocity component of the most unstable mode for different streamwise wavenumber α_v and a number of visualised sub-units n, chosen in both cases to give a good overview of the spatial characteristics of the mode. Isosurfaces correspond to $\pm 0.75 u_{max}$. Spanwise direction is normalised by the spatial period of a sub-unit $2\pi/||\mathbf{k}||$. Notice the beating phenomenon for $\alpha_v = 0$.

of the base flow, as for *type-I* modes. However, these are usually associated with non-zero streamwise wavenumber and higher frequencies.

In order to assess more precisely the nature of the $\alpha_v = 0$ mode, the amplitude A of the primary disturbance was varied. Figure 8 displays the evolution of the spectrum of the $\alpha_v = 0$ mode for different amplitudes. When $A \to 0$, characteristics of the primary instability are retrieved: the primary growth rate is reached for stationary cross-flow vortices. However, this mode results from the merging of two spatial branches, forming an exceptional point [29]. Exceptional points are spectral singularities in the parameter space of a system in which two or more eigenvalues, and their corresponding eigenvectors, simultaneously coalesce and are usually associated with strong interactions between modes like resonances [30]. In the present case, the exceptional point indicates the presence of interactions between cross-flow vortices with different spanwise wavenumbers as it can be seen for $A = 0.06$, from the two eigenfunctions

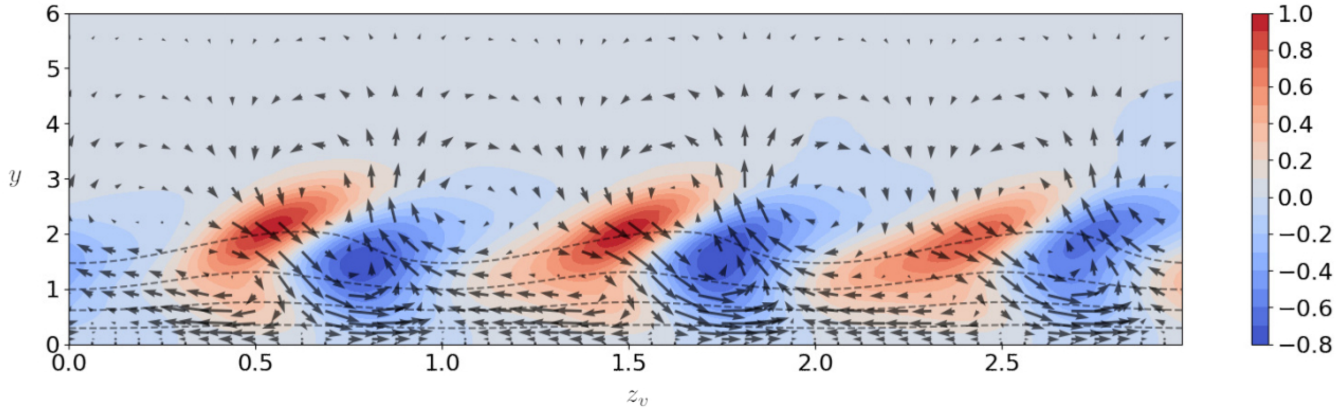

(a) $\alpha_v = 0$

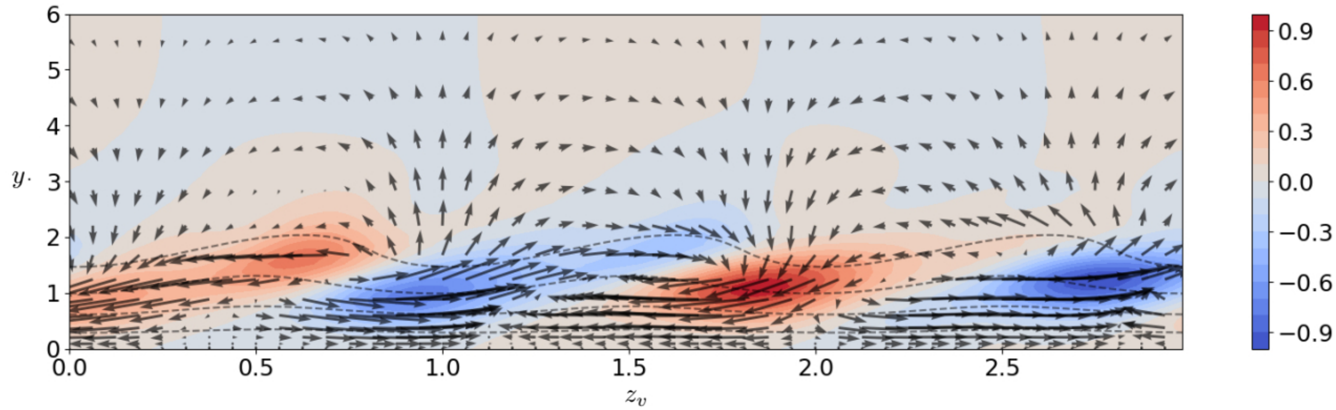

(b) $\alpha_v = 0.087$

FIG. 6: Vectors: cross-flow velocity in the plane (y, z_v) for a group of three sub-units. The contour plot represents the streamwise component of the secondary base flow. The flow in the z direction goes from left to right.

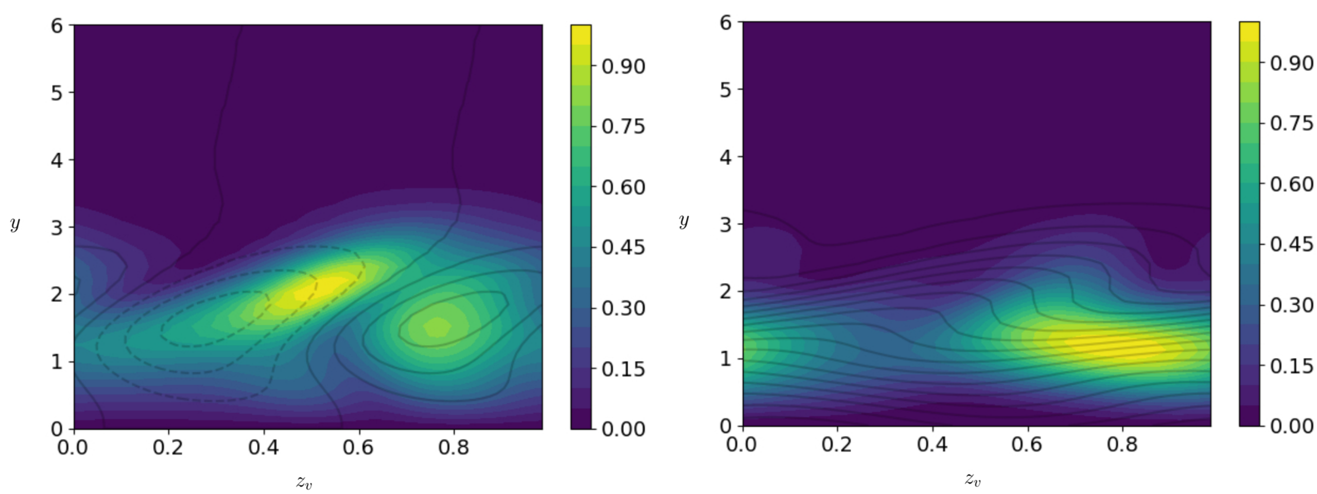

FIG. 7: Absolute value of the streamwise component of the eigenfunction for $\alpha_v = 0$ (left) and $\alpha_v = 0.087$ (right). The solid contours depict the spanwise and wall-normal velocity gradients of the secondary base flow, respectively.

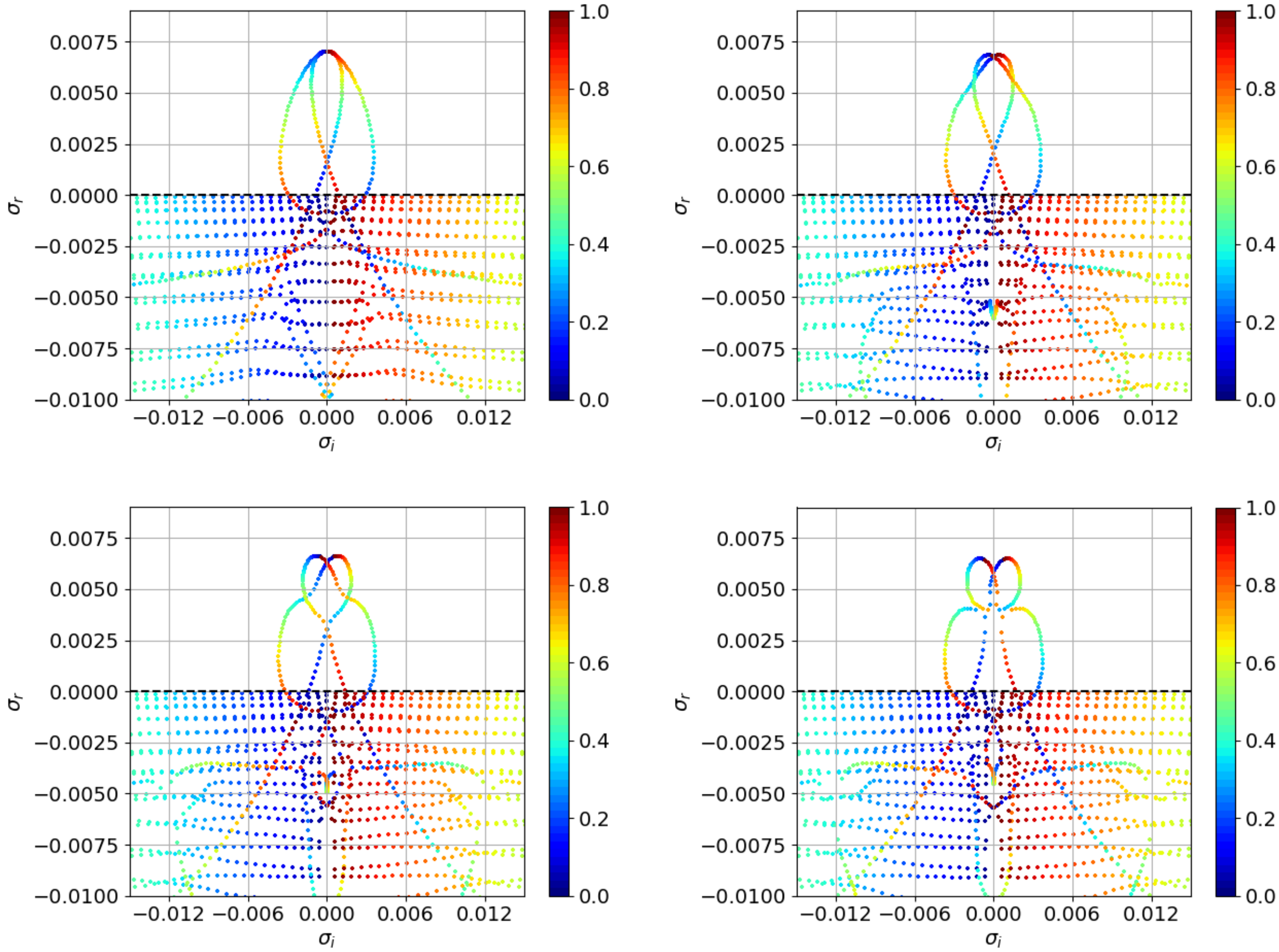

FIG. 8: Spectra of the secondary stability problem for $Re_\delta = 826$, $n = 50$, $\alpha_v = 0$ and for several amplitudes A. From left to right and top to bottom: $A = 0.02$, $A = 0.04$, $A = 0.06$ and $A = 0.07$. The dashed line corresponds to the $\sigma_r = 0$ line.

shown in figure 9. When the amplitude is increased, the outer branch is deformed, leading to the formation of two other exceptional points associated to interactions between travelling disturbances with opposite spanwise wavenumbers. For $A = 0.07$, a change in the topology of the spectrum can be observed: the two spatial branches break up, then reconnect in a different configuration, forming the loops observed in the spectrum of figure 4. This evolution of the spectrum tends to indicate a change in the nature of the modes. However, it may be noticed that the growth rate of this mode remains finite as the amplitude of the base flow primary instability continuously reduces to some small but finite threshold. Thus, the topological changes within the spectrum should be linked to the modulation effect provided by the increase in amplitude of the primary instability. The resulting eigenvectors are visualised together with the modulated base flow for $A = 0.02$ and $A = 0.07$.

On the contrary, carrying out the same analysis for the $\alpha_v = 0.087$ mode as shown in figure 10, only a continuous deformation of the unstable branch can be observed. Streamwise velocity eigenfunctions of the most unstable mode are provided in figure 11 for different amplitudes. The most unstable mode is found for $\epsilon \approx 0.35$ in all cases, yielding a secondary instability coupling approximately three sub-units. Besides, it appears to stem from a travelling cross-flow mode which is progressively deformed by the presence of the primary stationary cross-flow mode. The travelling cross-flow mode has a spatial periodicity approximately three times larger than the primary mode. This is in agreement with the findings of Malik *et al.* [31] who argued, using an NPSE approach, that the modulation is simply a result of the nonlinear interaction of the stationary and travelling disturbances that becomes more pronounced as the amplitude A is increased.

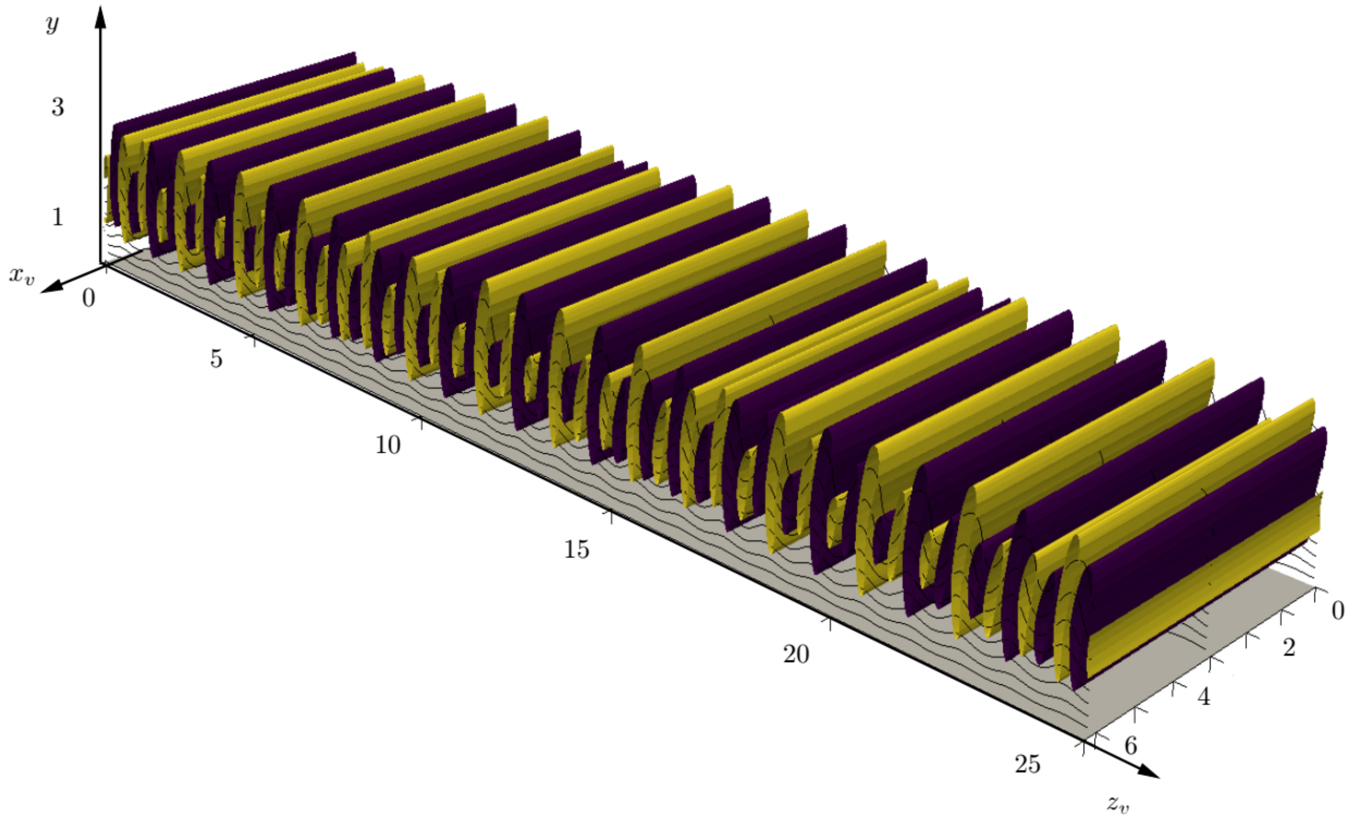

(a) ρ_{22}

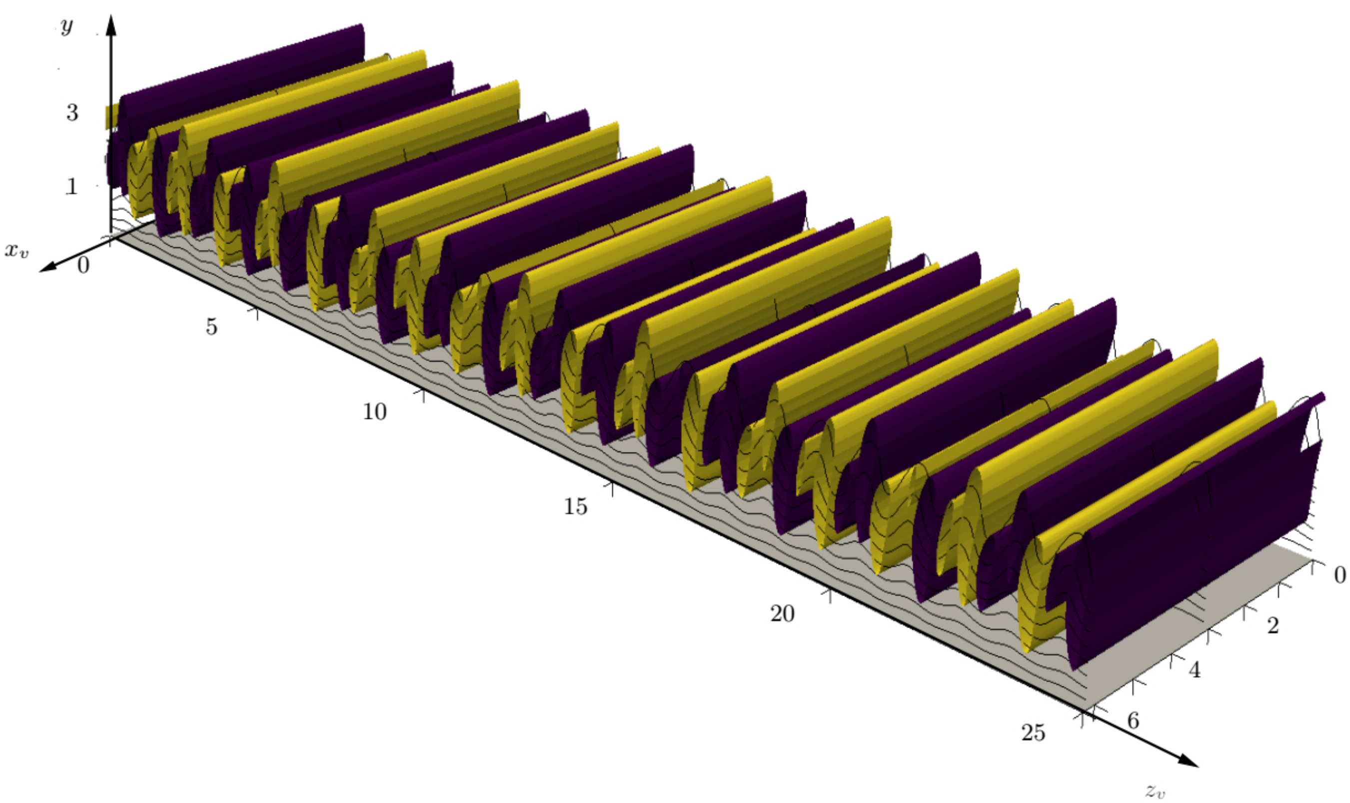

(b) ρ_{35}

FIG. 9: Three dimensional views of the streamwise velocity component of the unstable modes at the exceptional point for $\alpha_v = 0$, $A = 0.06$ and $n = 25$ sub-units. Isosurfaces correspond to $\pm 0.75 u_{max}$. The spanwise direction is normalised by the spatial period of a sub-unit $2\pi/||\mathbf{k}||$. Notice the beating phenomenon for $\alpha_v = 0$.

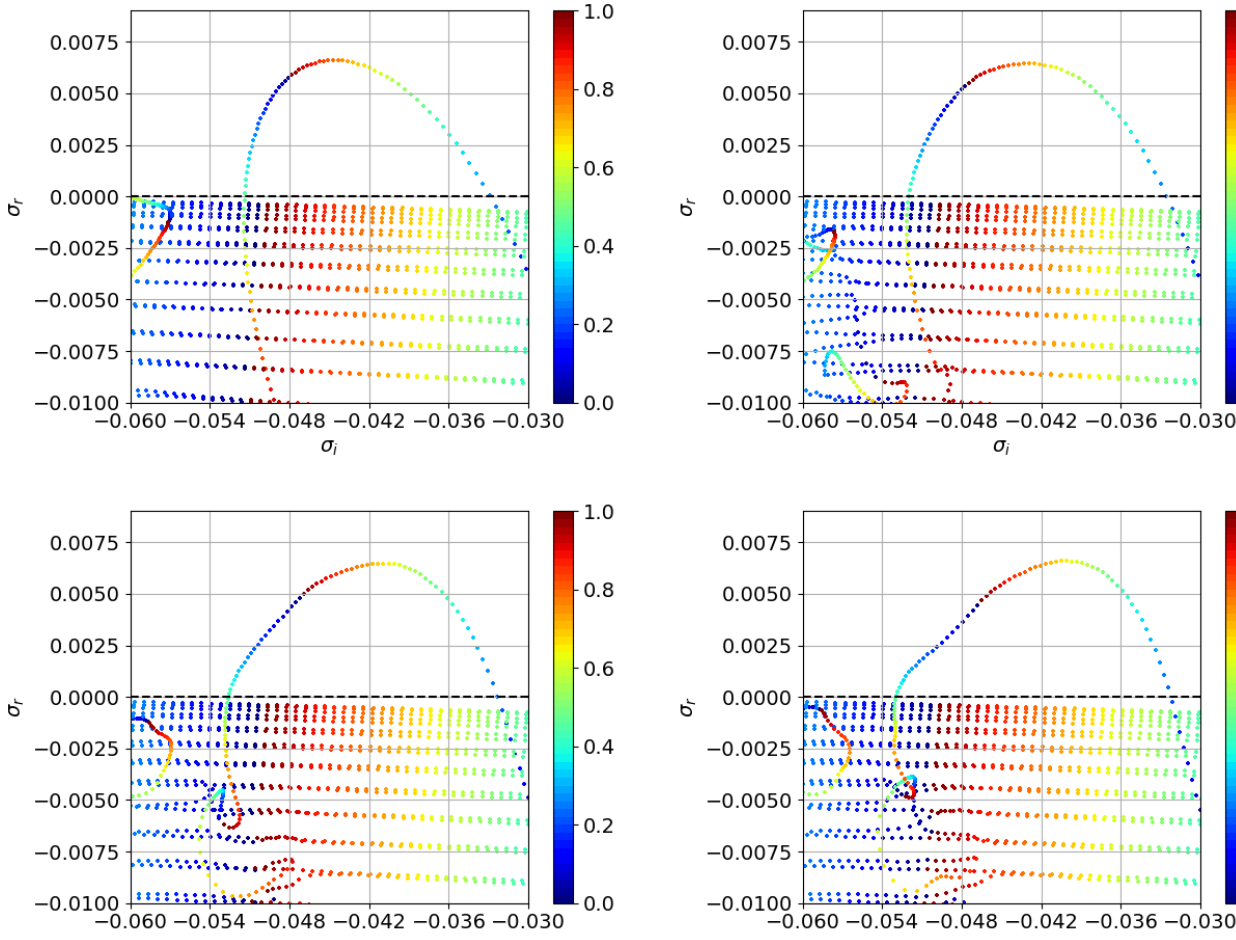

FIG. 10: Same as figure 8 but for the $\alpha_v = 0.087$ mode.

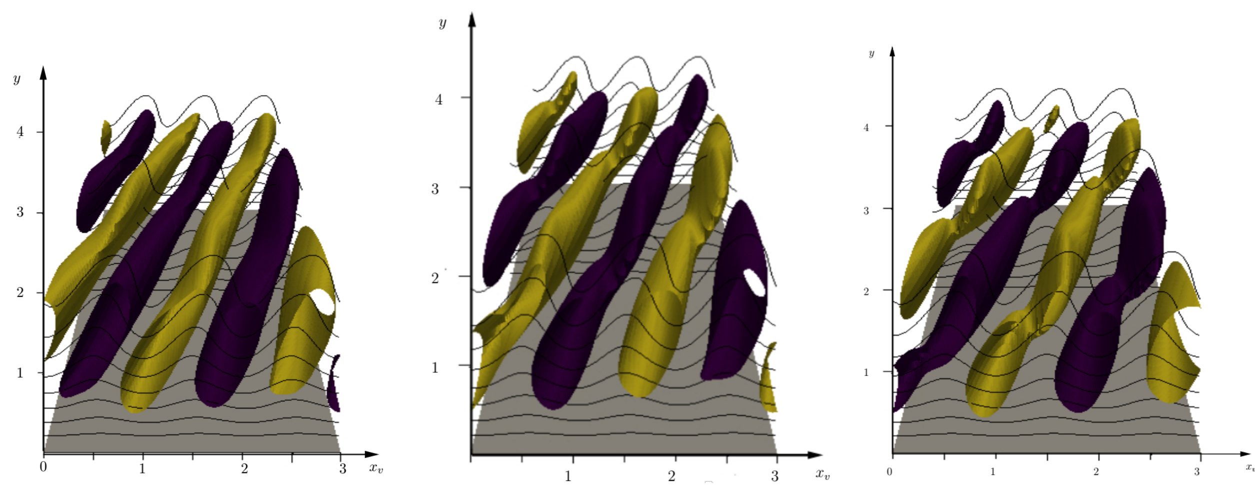

(a) $A = 0.02$ (b) $A = 0.06$ (c) $A = 0.07$

FIG. 11: Three dimensional views of the streamwise velocity perturbation of the most unstable mode for $\alpha_v = 0.087$ and different amplitudes. The number $n = 3$ of sub-units visualised has been chosen to accommodate approximately one spatial period of the secondary mode ($\epsilon \approx 0.35$). Isosurfaces correspond to $\pm 0.75 u_{max}$. Black contours represents the secondary base flow. The spanwise direction is normalised by the spatial period of a sub-unit $2\pi/||\mathbf{k}||$.

IV. CONCLUSIONS

A new formulation for secondary stability analysis of linearly unstable flows has been proposed, which allows retrieving amplification mechanisms involving detuned modes spanning several units of the primary instability. Such a method is based on the combination of a local two-dimensional stability analysis and a Bloch waves formalism originally described in Schmid *et al.* [1]. Within this framework, the linear stability of systems having a high number of degrees of freedom resulting from the repetition of several units of the primary instability, is investigated.

Using this method, the secondary stability of a swept boundary layer developing steady cross-flow vortices has been investigated. This flow case has been chosen due to previous observation of long-wavelength structures in numerical and experimental studies [16, 17], whose physical origin remained unclear. Moreover, for this flow case a direct comparison with the Floquet analysis carried out by the work of Fischer and Dallmann [2] (limited to small to intermediate wavelengths) can be made for validation. Here, we consider sub-units composed of one cross-flow stationary vortex, thus neglecting small mistunings between neighbouring vortices which might be responsible of mode localisation [32–34], potentially leading to high-amplitude phenomena like, for instance, the jagged aspect of the transition front. Within the same framework, this limitation can be partially overcame by considering sub-units composed of more than one cross-flow vortices, opportunely modulated in amplitude.

The instability dynamics seems to result from the competition between streamwise independent modes and detuned modes with detuning factor $\epsilon = 0.35$. In the case of streamwise wavenumbers $\alpha_v > 0.087$, the secondary instability analysis can be accurately described by a low number of modes and it has been previously retrieved by Floquet analysis. Whereas, for smaller wavenumbers, a multi-modal instability arises, corresponding to a Floquet mode with very small detuning factor, that has been never reported in the literature. The full spectra are retrieved, and unstable branches can be identified. Notably, for streamwise independent perturbations, large wavelengths oscillations can be seen, while a staggered pattern, characteristic of a subharmonic transition, appears in the disturbance for $\alpha_v = 0.087$. The wavelength of the staggered pattern is imposed by the detuning factor. Physically, two instability mechanisms have been identified: one linked to streaks and the circulation of high-momentum fluid towards the edge of the boundary layer. The other one appears linked to the roll-up of a shear layer and seems related to Kelvin-Helmholtz instabilities.

Notably, the obtained secondary disturbances show some similarities with the POD modes experimentally retrieved in the work of Serpieri and Kotsonis [17], Serpieri [28]. A direct comparison with these experimental findings has allowed to assess the nature of these secondary perturbations. In particular, the $\alpha_v = 0$ mode resembles a *type-I* mode, while the $\alpha_v = 0.087$ disturbance is clearly identified as a *type-III* mode which has been related to interactions between stationary and travelling cross-flow vortices. Often, this disturbance is considered as a modulation of the primary instability rather than a proper instability [31]. This possibility has been investigated by varying the amplitude of the primary disturbance: for the *type-III* mode, the unstable branch continuously deforms as the amplitude is increased. This approach has thus allowed the identification of two long-wavelength detuned instabilities that were observed in numerical and experimental literature studies. Some light has been shed on the dynamics of detuned secondary modes with small detuning factor, which have been overlooked in previous studies. However, they seem to play a role when the spatial wavelength of the secondary mode gets close to that of the base flow, yielding a long-wavelength beating phenomenon. It may be interesting to investigate the existence of detuned secondary instabilities of other canonical flows. In the case of cross-flow vortices, more accurate results could be obtained by using a nonlinearly saturated base flow. In general, studies on the secondary instability of fundamental coherent structures such as streaks could be completed and extended through the use of this framework.

V. APPENDIX

In this Appendix we carry out a sensitivity analysis of the results with respect to the main hypotheses of the method, namely the use of the finite number of subunits, and the neighbouring-coupling approach.
First, in order to verify that the limited number of subunits does not affect strongly the results, we have carried out our computations with increasing number of subunits. In figure 12 we show the eigenvalue spectra for the cases $\alpha_v = 0.03$ (top row) and $\alpha_v = 0.0087$ (bottom row) with $n = 50$ (left) and $n = 80$ (right) subunits. The spectra are practically identical. Thus, provided that the number of subunits is sufficiently high (here, $n > 50$), the finite number of subunits has virtually no effect on the results.
Concerning the nearest-neighbour coupling approach, we have increased for a few cases the number of coupled units, from $N_u = 3$ to $N_u = 50$. For the case $\alpha_v = 0.030$, which has $\rho = 0$ (fundamental instability) the growth rate does not change at all, as expected. For the detuned cases with $\alpha_v = 0.030$, $\rho = 48$ and $\alpha_v = 0.087$, $\rho = 30$, the maximum growth rate varies of 0.028% and 0.072%. Overall, we can say that the nearest-neighbour coupling approach has a

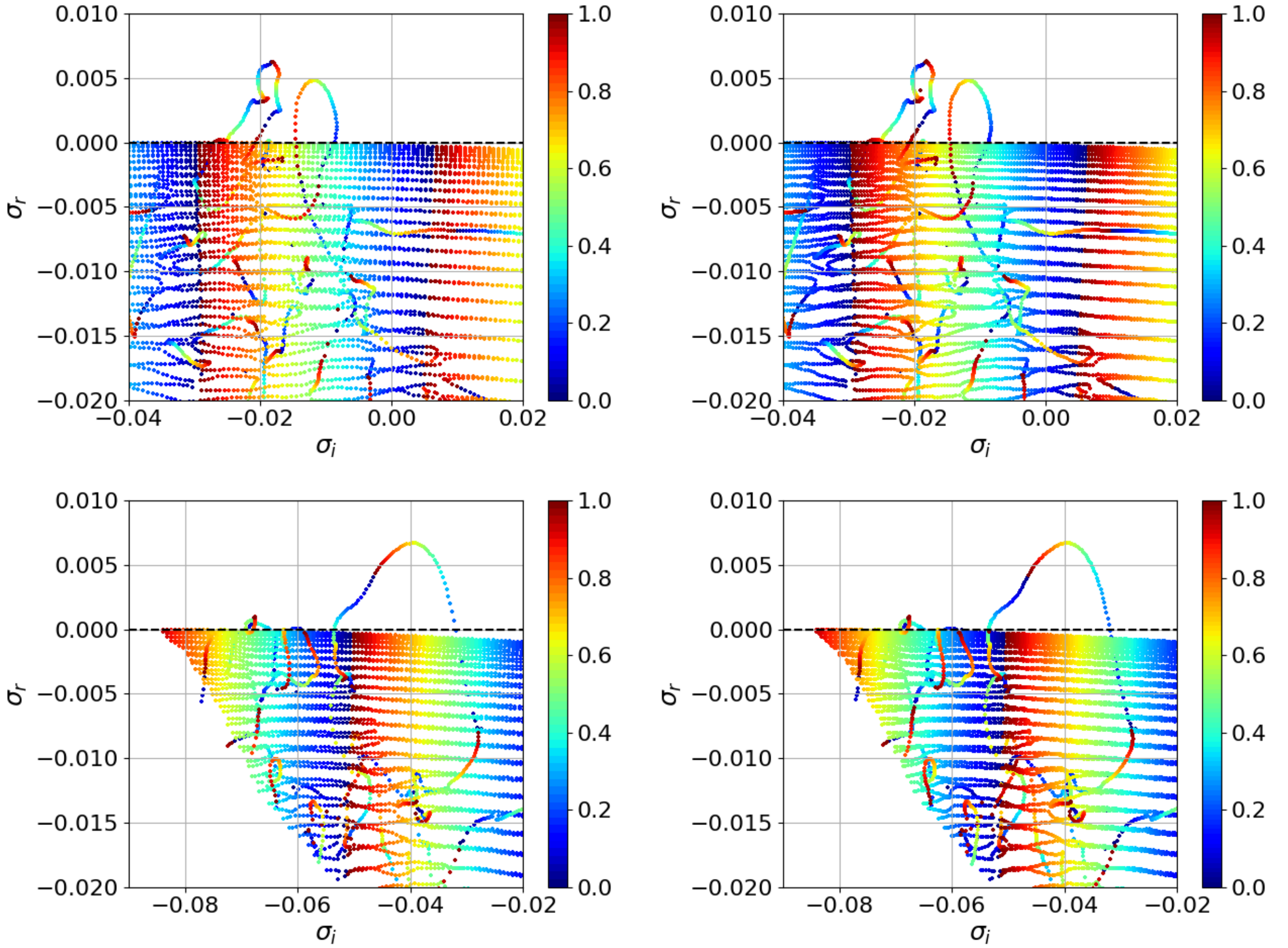

FIG. 12: Eigenvalues spectra for $Re_\delta = 826$, $A = 0.0789$, $\alpha_v = 0.03$ (top row) and $\alpha_v = 0.0087$ (bottom row) with a number of subunits (left) $n = 50$ and (right) $n = 80$. The dashed line corresponds to the $\sigma_r = 0$ line.

very slight effect on the results.

DECLARATION OF INTERESTS

The authors report no conflict of interest.

REFERENCES

[1] P. J. Schmid, M. F. de Pando, and N. Peake, Stability analysis for n-periodic arrays of fluid systems, Phys. Rev. Fluids **2**, 113902 (2017).

[2] T. M. Fischer and U. Dallmann, Primary and secondary stability analysis of a three-dimensional boundary-layer flow, Physics of Fluids A: Fluid Dynamics **3**, 2378 (1991), publisher: American Institute of Physics.

[3] P. J. Schmid and D. S. Henningson, *Stability and Transition in Shear Flows*, Applied Mathematical Sciences (New York, 2001).

[4] W. Tollmien, Über die entstehung der turbulenz, *Vorträge aus dem Gebiete der Aerodynamik und verwandter Gebiete*, , 18 (1930).

[5] L. M. Mack, enBoundary-Layer Linear Stability Theory, , 151 (1984).

[6] S. Chandrasekhar, The character of the equilibrium of an incompressible heavy viscous fluid of variable density, Mathematical Proceedings of the Cambridge Philosophical Society **51**, 162–178 (1955).

[7] S. C. Reddy and D. S. Henningson, Energy growth in viscous channel flows, Journal of Fluid Mechanics **252**, 209 (1993).

[8] S. A. Orszag and A. T. Patera, Secondary instability of wall-bounded shear flows, Journal of Fluid Mechanics **128**, 347–385 (1983).

[9] T. Herbert, enSecondary Instability of Plane Shear Flows — Theory and Application, in en*Laminar-Turbulent Transition*, International Union of Theoretical and Applied Mechanics, edited by V. V. Kozlov (Springer, Berlin, Heidelberg, 1985) pp. 9–20.

[10] Y. Liu, T. Zaki, and P. Durbin, Floquet analysis of secondary instability of boundary layers distorted by Klebanoff streaks and Tollmien-Schlichting waves 10.1063/1.3040302 (2008).

[11] G. Bonfigli and M. Kloker, enSecondary instability of crossflow vortices: validation of the stability theory by direct numerical simulation, Journal of Fluid Mechanics **583**, 229 (2007), publisher: Cambridge University Press.

[12] F. Picella, J. Robinet, and S. Cherubini, enOn the influence of the modelling of superhydrophobic surfaces on laminar–turbulent transition, Journal of Fluid Mechanics **901**, 10.1017/jfm.2020.516 (2020).

[13] P. Tabeling, O. Cardoso, and B. Perrin, Chaos in a linear array of vortices, Journal of Fluid Mechanics **213**, 511–530 (1990).

[14] C.-M. Ho and L.-S. Huang, Subharmonics and vortex merging in mixing layers, Journal of Fluid Mechanics **119**, 443–473 (1982).

[15] B. J. Olson, S. W. Shaw, C. Shi, C. Pierre, and R. G. Parker, Circulant Matrices and Their Application to Vibration Analysis, Applied Mechanics Reviews **66**, 10.1115/1.4027722 (2014).

[16] M. Högberg and D. Henningson, enSecondary instability of cross-flow vortices in Falkner–Skan–Cooke boundary layers, Journal of Fluid Mechanics **368**, 339 (1998), publisher: Cambridge University Press.

[17] J. Serpieri and M. Kotsonis, Three-dimensional organisation of primary and secondary crossflow instability, Journal of Fluid Mechanics **799**, 200–245 (2016).

[18] W. Koch, B. F. P., A. Stolte, and S. Hein, Nonlinear equilibrium solutions in a three-dimensional boundary layer and their secondary instability, Journal of Fluid Mechanics **406**, 131 (2000).

[19] P. Wassermann and M. Kloker, Mechanisms and passive control of crossflow-vortex-induced transition in a three-dimensional boundary layer, Journal of Fluid Mechanics **456**, 49 (2002).

[20] J.-C. Loiseau, *Dynamics and global stability analysis of three-dimensional flows*, Ph.D. thesis, ENSAM (2014).

[21] L. N. Trefethen, *Spectral Methods in MATLAB*, Software, Environments and Tools (Society for Industrial and Applied Mathematics, 2000).

[22] V. Falkner and S. Skan, Lxxxv. solutions of the boundary-layer equations, The London, Edinburgh, and Dublin Philosophical Magazine and Journal of Science **12**, 865 (1931).

[23] J. Cooke, The boundary layer of a class of infinite yawed cylinders, in *Mathematical proceedings of the Cambridge philosophical society*, Vol. 46 (Cambridge University Press, 1950) pp. 645–648.

[24] B. Müller, Experimental study of the travelling waves in a three-dimensional boundary layer, in *Laminar-Turbulent Transition*, edited by D. Arnal and R. Michel (Springer Berlin Heidelberg, Berlin, Heidelberg, 1990) pp. 489–498.

[25] J. Pralits, E. Alinovi, and A. Bottaro, Stability of the flow in a plane microchannel with one or two superhydrophobic walls (2017).

[26] E. B. White and W. S. Saric, Secondary instability of crossflow vortices, Journal of Fluid Mechanics **525**, 275–308 (2005).

[27] P. Hall, The linear development of görtler vortices in growing boundary layers, Journal of Fluid Mechanics **130**, 41–58 (1983).

[28] J. Serpieri, en*Cross-Flow Instability*, Ph.D. thesis, Delft University of Technology (2018).

[29] T. Kato, en*Perturbation Theory for Linear Operators* (Springer-Verlag, New York, 1995).

[30] W. D. Heiss, The physics of exceptional points, Journal of Physics A: Mathematical and Theoretical **45**, 444016 (2012).

[31] M. R. Malik, F. Li, and C.-L. Chang, Crossflow disturbances in three-dimensional boundary layers: nonlinear development, wave interaction and secondary instability, Journal of Fluid Mechanics **268**, 1–36 (1994).

[32] S.-T. Wei and C. Pierre, Localization Phenomena in Mistuned Assemblies with Cyclic Symmetry Part I: Free Vibrations, Journal of Vibration, Acoustics, Stress, and Reliability in Design **110**, 429 (1988).

[33] S.-T. Wei and C. Pierre, Localization Phenomena in Mistuned Assemblies with Cyclic Symmetry Part II: Forced Vibrations, Journal of Vibration, Acoustics, Stress, and Reliability in Design **110**, 439 (1988).

[34] A. Orchini, C. F. Silva, G. A. Mensah, and J. P. Moeck, Thermoacoustic modes of intrinsic and acoustic origin and their interplay with exceptional points, Combustion and Flame **211**, 83 (2020).